CHINESE OPTICS LETTERS

Vol. 19, No. 7 | July 2021

Scattering-amplitude phase in spiderlike photoelectron momentum distributions

Jiu Tang (唐 久), Guizhong Zhang (张贵忠)*, Yufei He (何宇飞), Xin Ding (丁 欣), and Jianquan Yao (姚建铨)

College of Precision Instrument and Optoelectronics Engineering, Tianjin University; Key Laboratory of Optoelectronic Information Technology, Ministry of Education, Tianjin 300072, China

*Corresponding author: johngzhang@tju.edu.cn

Received August 24, 2020 | Accepted December 5, 2020 | Posted Online March 16, 2021

The spiderlike structures in the photoelectron momentum distributions of ionized electrons from the hydrogen atom are numerically simulated by using a semiclassical rescattering model (SRM) and solving the time-dependent Schrödinger equation (TDSE), focusing on the role of the phase of the scattering amplitude. With the SRM, we find that the spiderlike legs shift to positions with smaller transverse momentum values while increasing the phase. The spiderlike patterns obtained by SRM and TDSE are in good agreement upon considering this phase. In addition, the time differences in electron ionization and rescattering calculated by SRM and the saddle-point equations are either in agreement or show very similar laws of variation, which further corroborates the significance of the phase of the scattering amplitude.

Keywords: photoelectron holography; semiclassical rescattering model; spiderlike structure.

DOI: 10.3788/COL202119.073201

1. Introduction

When an atom interacts with intense laser field[1], electrons will be ionized from the parent ion[2,3]. After tunneling ionization, some electrons leave the parent ion and reach the detector directly, and some electrons are driven back to the parent ion by the laser field and then rescatter off the parent ion. In fact, these two kinds of electrons will give rise to interference in the final photoelectron momentum distributions (PMDs) when their final momenta are equal, and these electrons are also named the reference beam and the signal beam, respectively. The interference process has also been referred to as strong-field photoelectron holography (SFPH)[4], a novel quantum analog of optical holography containing structural and dynamic information in PMDs[5–7]. Being an SFPH, the spiderlike structure in PMDs has been extensively investigated both experimentally and theoretically[8–16]. In 2012, Hickstein *et al.*[13] intuitively demonstrated that the shape and feature of the spiderlike structure depend on the number of times an electron passes its parent ion before rescattering. Because the spatial and temporal information of both the parent ions and electrons is encoded, the interference patterns have been used to extract structural and dynamic information in recent investigation[17–21]. Particularly, the scattering amplitude, $f(p,\theta) = |f(p,\theta)|e^{i\alpha(p,\theta)}$, has been used to characterize the strength of a scattering process, where $\alpha(p,\theta)$ is the phase of the scattering amplitude induced by the rescattering of the photoelectron with the parent ion. This phase can be of great significance in atomic physics and elementary particle physics[22,23]. In strong-field physics, the phase of the scattering amplitude is related to the structural information encoded in SFPH. In 2016, Zhou *et al.*[14] utilized a screened Coulomb potential model to extract this phase, and little following research was reported.

In the paper, we present our numerical results on the role of the scattering-amplitude phase in the spiderlike structure by deploying the semiclassical rescattering model (SRM) for hydrogen atoms. With this model, we show that the primary spiderlike structure arises from the interference between the reference electrons and the signal electrons scattered on their first revisit. For comparison, we also present the spiderlike structure simulated by solving the time-dependent Schrödinger equation (TDSE). The simulations show that the interference patterns obtained from the SRM do not agree with the TDSE results if the phase of the scattering amplitude is neglected, and these patterns agree with each other if this phase is included. We find that the time difference between electron ionization and rescattering extracted from SRM agrees fairly well with that calculated from TDSE.

2. Numerical Methods

In order to study the role of phase in the scattering amplitude of the spiderlike structure, we deploy SRM, which is based on the classical recollision three-step model[24–29]. In our simulation,

the laser field is linearly polarized along the x axis (in atomic units, a.u.):

$$E(t) = E_0 \sin(\omega t). \tag{1}$$

In SRM, we assume that the initial velocity of the signal electron is zero (i.e., $v_x^{\mathrm{sig}} = v_y^{\mathrm{sig}} = 0$), while the initial velocity of the reference electron is assumed to be $v_x^{\mathrm{ref}} = 0$ and $v_y^{\mathrm{ref}} \neq 0$. At the rescattering time, t_c, the signal electron is driven back to its initial position [i.e., $x(t_c) = y(t_c) = 0$]. The rescattering time, t_c, can be obtained by solving the equation of motion:

$$\sin(\omega t_c) - \sin(\omega t_0^{\mathrm{sig}}) - \omega(t_c - t_0^{\mathrm{sig}})\cos(\omega t_0^{\mathrm{sig}}) = 0. \tag{2}$$

The signal electron is elastically scattered by the parent ion at an angle θ_c. In our simulation, the scattering angle θ_c is within the range of -90° to 90°. The final momentum of the signal electron can be written as

$$p_x = v_c \cos\theta_c - \frac{E_0}{\omega}\cos(\omega t_c), \tag{3}$$

$$p_y = v_c \sin\theta_c, \tag{4}$$

where v_c is the velocity of the signal electron at the rescattering time t_c. When the final momentum of the signal electron is equal to that of the reference electron, interference will occur. Given the final momentum value, the ionization time and the initial velocity of the reference electron can be obtained as

$$t_0^{\mathrm{ref}} = \frac{1}{\omega}[\arccos(-\omega p_x/E_0)], \tag{5}$$

$$v_y = p_y. \tag{6}$$

The phase of each trajectory is given by the classical action along the path:

$$S = \int_0^{\infty}\left[\frac{v^2(t)}{2} + I_p\right]\mathrm{d}t. \tag{7}$$

In our simulation, the phase difference is given by

$$\Delta\theta = \frac{1}{2}\int_{t_0^{\mathrm{ref}}}^{t_c} v_x^2\mathrm{d}t + \frac{1}{2}v_y^2(t_c - t_0^{\mathrm{ref}}) - \frac{1}{2}\int_{t_0^{\mathrm{sig}}}^{t_c} v_x^2\mathrm{d}t + I_p(t_0^{\mathrm{sig}} - t_0^{\mathrm{ref}}) + \alpha, \tag{8}$$

where α is the phase of the scattering amplitude, as suggested by the theory deciphering the spiderlike structure[14,15]. Equation (8) can be rewritten in a simple form[14,15]:

$$\Delta\theta = \frac{1}{2}p_y^2(t_c - t_0^{\mathrm{ref}}) + \alpha. \tag{9}$$

From Eq. (9), it is clear that information of $t_c - t_0^{\mathrm{ref}}$ and α is encoded in the interference patterns of the PMDs.

The t_c and t_0^{ref} can be approximately determined from the saddle-point equations[30]. The saddle-point equations for the signal electron are

$$\frac{[\boldsymbol{k} + \boldsymbol{A}(t_0^{\mathrm{sig}})]^2}{2} = -I_p, \tag{10}$$

$$(t_c - t_0^{\mathrm{sig}})\boldsymbol{k} = -\int_{t_0^{\mathrm{sig}}}^{t_c}\mathrm{d}t'\boldsymbol{A}(t'), \tag{11}$$

$$\frac{[\boldsymbol{k} + \boldsymbol{A}(t_c)]^2}{2} = \frac{[\boldsymbol{p} + \boldsymbol{A}(t_c)]^2}{2}, \tag{12}$$

and the saddle-point equation for the reference electron is

$$\frac{[\boldsymbol{p} + \boldsymbol{A}(t_0^{\mathrm{ref}})]^2}{2} = -I_p. \tag{13}$$

In Eqs. (10)–(13), $\boldsymbol{k}$ and $\boldsymbol{p}$ are the electron drift momentum and final momentum, respectively. I_p is the ionization potential of the hydrogen atom. $\boldsymbol{A}(t)$ is the vector potential. Equations (10) and (13) stand for energy conservation in the process of tunneling, Eq. (11) is the return condition of signal electron, and Eq. (12) stands for energy conservation when the signal electron rescatters off the parent ion.

In order to obtain the PMDs, we also numerically solve the TDSE. In the length gauge, the TDSE is written in the following form (in a.u.):

$$i\frac{\partial\psi(r,t)}{\partial t} = \left[-\frac{1}{2}\nabla^2 + V(r) + r\cdot E(t)\right]\psi(r,t), \tag{14}$$

where $V(r) = -1/\sqrt{r^2 + b}$ is the Coulomb potential softened to avoid singularity and to match the ionization potential of hydrogen. The soft parameter b is set to be 0.9.

We use the wavefunction-splitting technique to obtain the PMDs. The wavefunction-splitting technique allows us to reconstruct the external wavefunction in the momentum space and to calculate the photoelectron momentum spectra accurately[31]. According to the wavefunction-splitting technique, the total simulation space is divided into the inner region ($|r| < r_{\mathrm{in}}$), outer region ($r_{\mathrm{ex}} < |r| < r_M$), and overlapping region ($r_{\mathrm{ex}} < |r| < r_{\mathrm{in}}$). In the overlapping region, we use an absorbing function to obtain the internal wavefunction ψ_{in} and the external wavefunction ψ_{ex}. The absorbing function is chosen to be

$$V_{\mathrm{abs}}(r) = \frac{1}{1 + \exp\left(\frac{r - r_0}{\Delta r}\right)}. \tag{15}$$

The wavefunctions are related by the following form:

$$\psi_{\mathrm{in}}(r,t) = V_{\mathrm{abs}}(r)\psi(r,t), \tag{16}$$

$$\psi_{\mathrm{ex}}(r,t) = [1 - V_{\mathrm{abs}}(r)]\psi(r,t). \tag{17}$$

The final PMDs are obtained from the accumulated momentum-space external wavefunction.

3. Results and Discussion

In our numerical simulation, the intensity and wavelength of the laser pulses are varied around $I = 4 \times 10^{13}$ W/cm^2 and $\lambda = 2000$ nm, respectively. The absolute phase of the laser pulse is zero.

We use the Monte Carlo algorithm in the simulation by sampling electrons ionized within two optical cycles (o.c.), i.e., $[0, 2T]$. Our extensive simulation gives typical spiderlike interference structures, and we choose to show one with $\alpha = 0$ in Figs. 1(a)–1(c). In order to demonstrate the feasibility of SRM, we also numerically solve the TDSE to obtain the spiderlike structure, as given in Figs. 1(d)–1(f). One can discern three types of interference patterns in the momentum distributions[32–35]: co-circular rings, short arcs, and spiderlike features. Corresponding to Figs. 1(a)–1(c), we show the reference trajectory and the signal trajectory contributing to the spiderlike feature in Fig. 1(g). We focus on the spiderlike structure in our discussion. One can observe that the spiderlike features in Figs. 1(a)–1(c) resemble those of the TDSE result in Figs. 1(d)–1(f), proving that the overall features obtained by the TDSE are reproduced by the SRM. Therefore, we can use SRM to retrieve the time and spatial information encoded in the holographic spiderlike structure. For making a quantitative comparison, we show, in Fig. 1(h), the cut-plot curves taken along the transverse (p_y axis) direction at a given longitudinal momentum (at fixed p_x) in the spiderlike patterns of Figs. 1(a)–1(f). One sees that these two curves do not overlap with each other, which may be attributed to the absence of the Coulomb potential in SRM[27,28]. However, they will overlap if a proper non-zero value of phase α is used in the SRM simulation.

In order to reveal the role of the phase of the scattering amplitude, α, in the spiderlike structure and possibly in other interference patterns, we assume that α is a constant up to a zeroth-order approximation. In Figs. 2(a)–2(g), we chose to show some typical spiderlike patterns for $\alpha = 0$, $\pi/20$, $\pi/10$, $3\pi/20$, $\pi/5$, $\pi/4$, and $3\pi/10$, and several cut-plot curves at $p_x = 4.0$ a.u. in Fig. 2(h). These cut-plot curves are the transverse momentum distributions manifesting that the spiderlike patterns are gradually narrowing in the transverse direction, and the intensities of the zeroth-order interference maxima (central maxima) are decreasing when α is increased from zero to $3\pi/10$. This observation is in agreement with the theoretical prediction of Eq. (9). We take the first interference minimum in the transverse momentum distributions (cut-plot curves) for discussion. Equation (12) can be solved for the transverse momentum values corresponding to the first transverse minimum as $p_y = \sqrt{2(\pi - \alpha)/(t_c - t_0^{\text{ref}})}$. It can be seen that the position of the first interference minimum depends on the value of α, and p_y will decrease when α increases. As a result, the first interference minimum unambiguously shifts to positions with

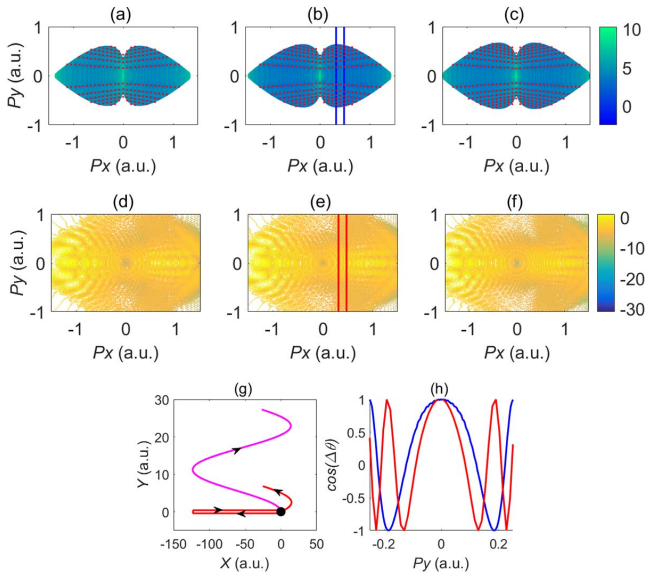

Fig. 1. Photoelectron momentum distributions of hydrogen atoms simulated by (a)–(c) the semiclassical rescattering model (SRM, α is set to zero; red dots on the interference minima are just for guiding the eyes) and (d)–(f) TDSE. Because there are not many optical cycles in the pulse, the TDSE results are asymmetric with respect to the $p_x = 0$ axis. The top two panels correspond to wavelengths of (a), (d) $\lambda = 1900$ nm, (b), (e) $\lambda = 2000$ nm, and (c), (f) $\lambda = 2100$ nm, respectively. (g) Typical trajectories that form the spiderlike structure in the SRM: the parent ion is at the origin of the axis. The pink curve is the reference trajectory, and the red curve is the signal trajectory. A scattering angle of 5° is assumed for the signal trajectory. (h) Cut-plot curves taken at $p_x = 0.4$ a.u. for the SRM (blue) and TDSE (red), and the cut positions are marked by the colored vertical lines in (b) and (e). Intensity of the laser pulse is $I = 4 \times 10^{13}$ W/cm^2, and the pulse duration is two optical cycles.

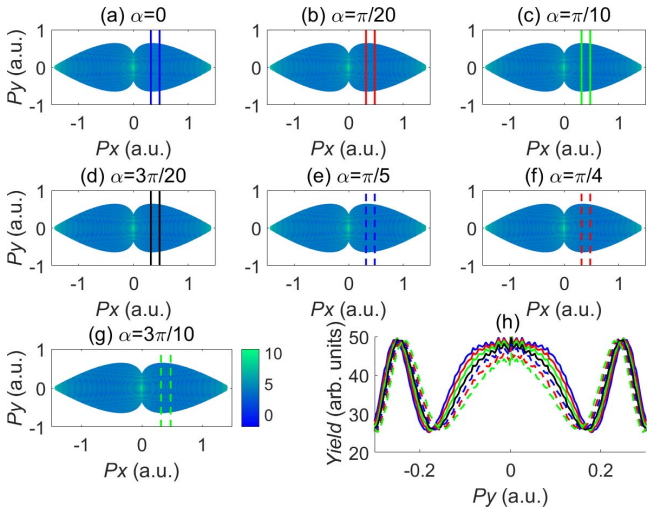

Fig. 2. Spiderlike structures numerically obtained by the SRM. The patterns correspond to phase values of (a) $\alpha = 0$, (b) $\pi/20$, (c) $\pi/10$, (d) $3\pi/20$, (e) $\pi/5$, (f) $\pi/4$, and (g) $3\pi/10$, respectively. (h) Cut-plot curves are taken at $p_x = 0.4$ a.u. from the spiderlike patterns in (a) (blue solid curve), (b) (red solid curve), (c) (green solid curve), (d) (black solid curve), (e) (blue dotted curve), (f) (red dotted curve), and (g) (green dotted curve), respectively. The cut positions are marked by the colored vertical lines in (a)–(g). The laser parameters are the same as in Fig. 1.

smaller transverse momentum values. These analyses demonstrate that the phase α induced by Coulomb interaction of the signal electron with the parent ion plays an important role in the spiderlike patterns. In addition, Fig. 2(h) shows that the intensities of the zeroth-order interference maxima decrease when α increases. However, the reduction of the zeroth-order interference maxima was not reported before, possibly because the phase α is small at low momentum and small scattering angle, and the fact that the SRM does not consider the amplitudes of the signal and the reference electrons.

For investigating the time information pertaining to ionization and rescattering, we use a window function[14] to average the interference fringes over p_x in a narrow interval $p_x \pm \Delta p_x$ for a better signal-to-noise ratio and a curve-fitting procedure for the cut-plot curves. By choosing the cut position of $p_x = 0.4$ a.u. and a suitable window width of $\Delta p_x = 0.08$ a.u., we obtain several cut-plot curves of the interference structures at the fixed p_x. Then, we use the curve-fitting procedure to extract the interference term $\cos(\Delta\theta)$ from these curves. The quantities $t_c - t_0^{\text{ref}}$ and α encoded in these spiderlike structures are extracted from the interference term $\cos(\Delta\theta)$ by using Eq. (9). Figure 3(b) presents quantity $t_c - t_0^{\text{ref}}$ extracted by fitting the cut-plot curves [like those in Fig. 2(h)]; it is clear that the extracted $t_c - t_0^{\text{ref}}$ decreases with the increasing final momentum p_x. Then, we compare the extracted $t_c - t_0^{\text{ref}}$ with the calculated $t_c - t_0^{\text{ref}}$ by the saddle-point equations[30] and show them in Fig. 3(b). Their excellent agreement further demonstrates that this time difference is not the main reason for the disparity of the interference patterns obtained by SRM and TDSE. Quantities $t_c - t_0^{\text{ref}}$ extracted by fitting to Eq. (9) and calculated from the saddle-point equations both deviate obviously from the quantity $t_c - t_0^{\text{ref}}$ obtained directly by the SRM. Nevertheless, the time difference obtained by these three methods manifests a similar law of linear variation with the final momentum p_x. This monotonic variation of $t_c - t_0^{\text{ref}}$ with p_x can explain the shift of the spiderlike feature: with increasing p_x, $t_c - t_0^{\text{ref}}$ decreases, leading to an increase of the p_y value at which the first interference minimum is located. As a result, the spiderlike structures become thinner for smaller longitudinal momenta, which are in agreement with the appearance of the interference patterns in Figs. 1(a)–1(f).

We also monitor variations of higher-order interference fringes, or more spider legs, with the phase by studying how the positions, or the transverse momentum values at which the first, second, and third interference minima are located, shift with α. To that end, we obtain the cut-plot curves at a cut position of $p_x = 0.4$ a.u. in the spiderlike patterns [as shown in Fig. 4(a)], then we compare the interference minimum positions, $p_y^{\min}$, extracted by fitting to Eq. (9) with that calculated from the SRM, and the result is shown in Fig. 4(b). It is obvious that these two kinds of $p_y^{\min}$ values are in good agreement because the phase α is taken into account. With the increase of the phase of the scattering amplitude, the position of the interference minimum decreases to smaller transverse momenta, and thus the shift of the spiderlike structure becomes appreciable, which corroborates our previous analysis on the first interference minimum. These observations also reveal that SRM is powerful in elucidating SFPH.

To further study the impact of the phase of the scattering amplitude in the spiderlike structure, we use a fitting algorithm[14] to extract the value of phase α from the cut-plot curves of the spiderlike patterns simulated by TDSE, and the results are presented in Fig. 5(a). One can see that α is close to zero when $p_y = 0$ a.u., and thus the zeroth-order interference maximum will not decrease in intensity. Then, we use the value of phase α extracted from the TDSE results to obtain a modified cut-plot curve of the spiderlike structure simulated by SRM combining with Eq. (9), and this curve is given in Fig. 5(b). Clearly, the

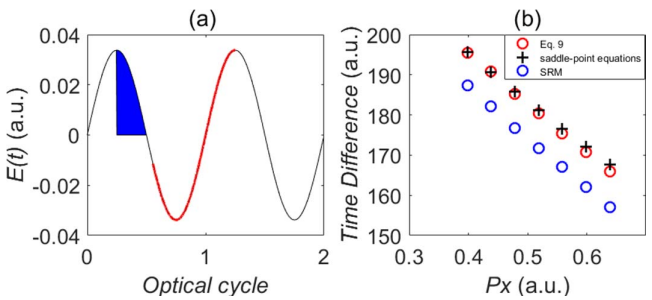

Fig. 3. (a) Blue area presents the tunneling time range of signal electron wavepackets and reference electron wavepackets involved in the spiderlike structures. The red curve presents the rescattering time range of signal electron wavepackets. (b) Variations of the time difference between rescattering of the signal electron and ionization of the reference electron with p_x. The red circles, blue circles, and black pluses represent the time difference extracted by fitting the cut-plot curves of the spiderlike structure using Eq. (9), the time differences obtained by the SRM, and the time differences calculated by the saddle-point equations, respectively.

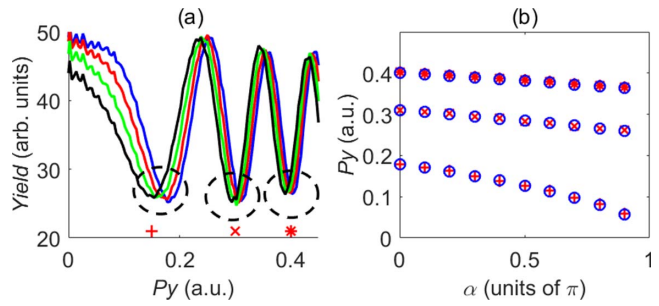

Fig. 4. (a) Cut-plot curves are taken at $p_x = 0.4$ a.u. from the spiderlike patterns corresponding to $\alpha = 0$ (blue curve), $\pi/10$ (red curve), $\pi/5$ (green curve), and $3\pi/10$ (black curve), respectively. The first, second, and third interference minimum positions are marked by black dotted circles. (b) Variations of the interference minimum positions (values of transverse momenta or p_y) of the cut-plot curves taken at $p_x = 0.4$ a.u. with α. The first, second, and third interference minimum positions calculated using Eq. (9) are marked by blue circles. For comparison, the corresponding positions calculated by the SRM are shown by red pluses, red crosses, and red star symbols.

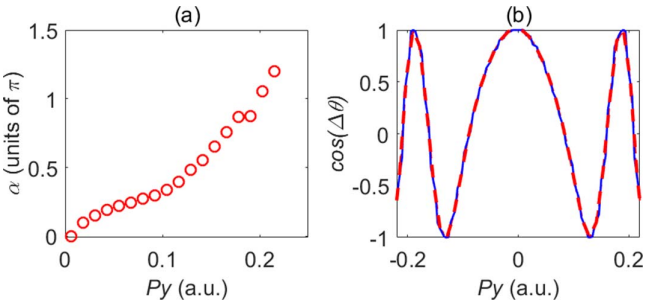

Fig. 5. (a) Values of phase α extracted from the cut-plot curves simulated by TDSE, plotted as a function of p_y. (b) Cut-plot curves taken at $p_x = 0.4$ a.u. The red dashed curve represents the curve obtained from TDSE. The blue solid curve represents the modified results of Fig. 1(a) after considering a phase value given in Fig. 5(a) in SRM.

modified curve agrees well with that obtained by the TDSE, simply because we have included both the phase difference between the signal electron and the reference electron accumulated during their propagation and the phase of the scattering amplitude.

4. Conclusion

In summary, by deploying SRM for hydrogen atoms, we have successfully simulated the spiderlike structure in PMDs and proven that the spiderlike structure well reproduces that by TDSE upon considering the phase of the scattering amplitude. Analyses on the cut-plot curves taken from the spiderlike patterns for interrogating the role of the phase have demonstrated their significance in deciphering the spiderlike interference patterns. Our simulation shows that the spiderlike feature shifts to positions of smaller transverse momentum values with increasing α. The time differences in electron ionization and rescattering calculated by SRM and the saddle-point equations are either in agreement or show similar laws of linear variation, thus strengthening the reliability of the SRM and corroborating the significance of the phase of the scattering amplitude in spiderlike PMDs.

Acknowledgement

This research was supported by the National Natural Science Foundation of China (Nos. 11674243 and 11674242) and the State Key Research Program Grant (No. 2017YFB1401201).

References

1. X. Wang, X. Yan, K. Jin, Y. Dai, Z. Jin, X. Yang, and G. Ma, "Generation of femtosecond dual pulses by a transverse standing wave in a volume holographic grating," Chin. Opt. Lett. **17**, 113201 (2019).
2. M. Peng and L. Bai, "Scaling law in nonsequential double ionization by counter-rotating two-color circularly polarized laser fields," Chin. Opt. Lett. **18**, 110201 (2020).
3. Z. Xiao, W. Quan, S. Xu, S. Yu, Y. Wang, M. Zhao, M. Wei, Y. Zhou, X. Lai, J. Chen, and X. Liu, "Coulomb potential influence in the attoclock experimental scheme," Chin. Opt. Lett. **18**, 010201 (2020).
4. H. Xie, M. Li, S. Luo, Y. Li, J. Tan, Y. Zhou, W. Cao, and P. Lu, "Photoelectron holography and forward scattering in atomic ionization by elliptically polarized laser pulses," Opt. Lett. **43**, 3220 (2018).
5. M. Spanner, O. Smirnova, P. B. Corkum, and M. Yu Ivanov, "Reading diffraction images in strong field ionization of diatomic molecules," J. Phys. B **37**, L243 (2004).
6. M. He, Y. Li, Y. Zhou, M. Li, and P. Lu, "Temporal and spatial manipulation of the recolliding wave packet in strong-field photoelectron holography," Phys. Rev. A **93**, 033406 (2016).
7. Y. Huismans, A. Rouzée, A. Gijsbertsen, J. H. Jungmann, A. S. Smolkowska, P. S. W. M. Logman, F. Lépine, C. Cauchy, S. Zamith, T. Marchenko, J. M. Bakker, G. Berden, B. Redlich, A. F. G. van der Meer, H. G. Muller, W. Vermin, K. J. Schafer, M. Spanner, M. Y. Ivanov, O. Smirnova, D. Bauer, S. V. Popruzhe, and M. J. J. Vrakking, "Time-resolved holography with photoelectrons," Science **331**, 61 (2011).
8. X.-B. Bian and A. D. Bandrauk, "Attosecond time-resolved imaging of molecular structure by photoelectron holography," Phys. Rev. Lett. **108**, 263003 (2012).
9. M. Meckel, A. Staudte, S. Patchkovskii, D. M. Villeneuve, P. B. Corkum, R. Dörner, and M. Spanner, "Signatures of the continuum electron phase in molecular strong-field photoelectron holography," Nat. Phys. **10**, 594 (2014).
10. M. Liu, M. Li, C. Wu, Q. Gong, A. Staudte, and Y. Liu, "Phase structure of strong-field tunneling wave packets from molecules," Phys. Rev. Lett. **116**, 163004 (2016).
11. M. Haertelt, X. Bian, M. Spanner, A. Staudte, and P. B. Corkum, "Probing molecular dynamics by laser-induced backscattering holography," Phys. Rev. Lett. **116**, 133001 (2016).
12. J. Tan, Y. Zhou, M. Li, M. He, Y. Liu, and P. Lu, "Accurate measurement of laser intensity using photoelectron interference in strong-field tunneling ionization," Opt. Express **26**, 20063 (2018).
13. D. D. Hickstein, P. Ranitovic, S. Witte, X. Tong, Y. Huismans, P. Arpin, X. Zhou, K. Ellen Keister, C. W. Hogle, B. Zhang, C. Ding, P. Johnsson, N. Toshima, M. J. J. Vrakking, M. M. Murnane, and H. C. Kapteyn, "Direct visualization of laser-driven electron multiple scattering and tunneling distance in strong-field ionization," Phys. Rev. Lett. **109**, 073004 (2012).
14. Y. Zhou, O. I. Tolstikhin, and T. Morishita, "Near-forward rescattering photoelectron holography in strong-field ionization: extraction of the phase of the scattering amplitude," Phys. Rev. Lett. **116**, 173001 (2016).
15. J. Tan, Y. Zhou, M. He, Y. Chen, Q. Ke, J. Liang, X. Zhu, M. Li, and P. Lu, "Determination of the ionization time using attosecond photoelectron interferometry," Phys. Rev. Lett. **121**, 253203 (2018).
16. Q. Z. Xia, J. F. Tao, J. Cai, L. B. Fu, and J. Liu, "Quantum interference of glory rescattering in strong-field atomic ionization," Phys. Rev. Lett. **121**, 143201 (2018).
17. Y. Huismans, A. Gijsbertsen, A. S. Smolkowska, J. H. Jungmann, A. Rouzée, P. S. W. M. Logman, F. Lépine, C. Cauchy, S. Zamith, T. Marchenko, J. M. Bakker, G. Berden, B. Redlich, A. F. G. van der Meer, M. Y. Ivanov, T.-M. Yan, D. Bauer, O. Smirnova, and M. J. J. Vrakking, "Scaling laws for photoelectron holography in the midinfrared wavelength regime," Phys. Rev. Lett. **109**, 013002 (2012).
18. A. S. Maxwell, A. Al-Jawahiry, X. Y. Lai, and C. Figueira de Morisson Faria, "Analytic quantum-interference conditions in Coulomb corrected photoelectron holography," J. Phys. B **51**, 044004 (2018).
19. M. He, Y. Li, Y. Zhou, M. Li, W. Cao, and P. Lu, "Direct visualization of valence electron motion using strong-field photoelectron holography," Phys. Rev. Lett. **120**, 133204 (2018).
20. J. Tan, Y. Zhou, M. He, Q. Ke, J. Liang, Y. Li, M. Li, and P. Lu, "Time-resolving tunneling ionization via strong-field photoelectron holography," Phys. Rev. A **99**, 033402 (2019).
21. M. Li, H. Xie, W. Cao, S. Luo, J. Tan, Y. Feng, B. Du, W. Zhang, Y. Li, Q. Zhang, P. Lan, Y. Zhou, and P. Lu, "Photoelectron holographic interferometry to probe the longitudinal momentum offset at the tunnel exit," Phys. Rev. Lett. **122**, 183202 (2019).
22. J. Schmiedmayer, M. S. Chapman, C. R. Ekstrom, T. D. Hammond, S. T. Wehinger, and D. E. Pritchard, "Index of refraction of various gases for sodium matter waves," Phys. Rev. Lett. **74**, 1043 (1995).
23. I. P. Ivanov, "Measuring the phase of the scattering amplitude with vortex beams," Phys. Rev. D **85**, 076001 (2012).

24. G. G. Paulus, W. Becker, W. Nicklich, and H. Walther, "Rescattering effects in above-threshold ionization: a classical model," J. Phys. B **27**, L703 (1994).
25. P. B. Corkum, "Plasma perspective on strong field multiphoton ionization," Phys. Rev. Lett. **71**, 1994 (1993).
26. X.-B. Bian, Y. Huismans, O. Smirnova, K.-J. Yuan, M. J. J. Vrakking, and A. D. Bandrauk, "Subcycle interference dynamics of time-resolved photoelectron holography with midinfrared laser pulses," Phys. Rev. A **84**, 043420 (2011).
27. H. Xie, M. Li, Y. Li, Y. Zhou, and P. Lu, "Intra-half-cycle interference of low-energy photoelectron in strong midinfrared laser fields," Opt. Express **24**, 27726 (2016).
28. M. Li, W. C. Jiang, H. Xie, S. Luo, Y. Zhou, and P. Lu, "Strong-field photoelectron holography of atoms by bicircular two-color laser pulses," Phys. Rev. A **97**, 023415 (2018).
29. S. Brennecke, N. Eicke, and M. Lein, "Gouy's phase anomaly in electron waves produced by strong-field ionization," Phys. Rev. Lett. **124**, 153202 (2020).
30. P. Salières, B. Carré, L. Le Déroff, F. Grasbon, G. G. Paulus, H. Walther, R. Kopold, W. Becker, D. B. Milošević, A. Sanpera, and M. Lewenstein, "Feynman's path-integral approach for intense-laser-atom interactions," Science **292**, 902 (2001).
31. S. Chelkowski, C. Foisy, and A. D. Bandrauk, "Electron-nuclear dynamics of multiphoton H^{2+} dissociative ionization in intense laser fields," Phys. Rev. A **57**, 1176 (1998).
32. D. G. Arbó, K. L. Ishikawa, K. Schiessl, E. Persson, and J. Burgdörfer, "Intracycle and intercycle interferences in above-threshold ionization: the time grating," Phys. Rev. A **81**, 021403 (2010).
33. D. G. Arbó, E. Persson, and J. Burgdörfer, "Time double-slit interferences in strong-field tunneling ionization," Phys. Rev. A **74**, 063407 (2006).
34. F. Lindner, M. G. Schätzel, H. Walther, A. Baltuška, E. Goulielmakis, F. Krausz, D. B. Milosević, D. Bauer, W. Becker, and G. G. Paulus, "Attosecond double-slit experiment," Phys. Rev. Lett. **95**, 040401 (2005).
35. M. Richter, M. Kunitski, M. Schöffler, T. Jahnke, L. P. H. Schmidt, M. Li, Y. Liu, and R. Dörner, "Streaking temporal double-slit interference by an orthogonal two-color laser field," Phys. Rev. Lett. **114**, 143001 (2015).